

Solid-State NMR Investigation of the Dynamics of the Soluble and Membrane-Bound Colicin Ia Channel-Forming Domain[†]

Daniel Huster, Linshi Xiao, and Mei Hong*

Department of Chemistry, Iowa State University, Ames, Iowa 50011

Received November 28, 2000; Revised Manuscript Received March 28, 2001

ABSTRACT: Solid-state NMR spectroscopy was employed to study the molecular dynamics of the colicin Ia channel domain in the soluble and membrane-bound states. In the soluble state, the protein executes small-amplitude librations (with root-mean-square angular fluctuations of 0–10°) in the backbone and larger-amplitude motions (16–17°) in the side chains. Upon membrane binding, the motional amplitudes increase significantly for both the backbone (12–16°) and side chains (23–29°), as manifested by the reduction in the C–H and H–H dipolar couplings and ¹⁵N chemical shift anisotropy. These motions occur not only on the pico- to nanosecond time scales, but also on the microsecond time scale, as revealed by the ¹H rotating-frame spin-lattice relaxation times. Average motional correlation times of 0.8 and 1.2 μs were extracted for the soluble and membrane-bound states, respectively. In comparison, both forms of the colicin Ia channel domain are completely immobile on the millisecond scale. These results indicate that the colicin Ia channel domain has enhanced conformational mobility in the lipid bilayer compared to the soluble state. This membrane-induced mobility increase is consistent with the loss of tertiary structure of the protein in the membrane, which was previously suggested by the extended helical array model [Zakharov et al. (1998) *Proc. Natl. Acad. Sci. U.S.A.* 95, 4282–4287]. An extended structure would also facilitate protein interactions with the mobile lipids and thus increase the protein internal motions. We speculate that the large mobility of the membrane-bound colicin Ia channel domain is a prerequisite for channel opening in the presence of a voltage gradient.

It has long been recognized that molecular dynamics play an important role in biological functions such as protein folding, target recognition, conformational exchange, protein–protein interaction, and complex formation. Protein dynamics cover a wide range of time scales from picoseconds to seconds and exhibit varying amplitudes and geometries such as small-amplitude librations, aromatic ring flips, aliphatic side chain discrete jumps, and methyl group rotations. Much of the recent progress in the study of protein dynamics comes from solution NMR relaxation time measurements, which can be used to probe fast and intermediate time scale motions of globular proteins (1–3). A great deal of interest also exists in the molecular dynamics of membrane-bound proteins. For instance, dynamic conformational changes are important for the opening and closing of ion channel proteins (4–9) and for the activation of transmembrane receptor proteins (10).

Channel-forming colicins are bactericidal proteins that are water-soluble but have a strong propensity to insert spontaneously into the inner membrane of sensitive bacterial cells (11, 12). The membrane-inserted structure of colicins corresponds to an intermediate state in the pathway toward the opening of the channel in the presence of a voltage gradient (11–14). While the soluble structure of many members of the colicin family is known from crystallography, relatively

little information is available on the dynamics of either the membrane-bound or the soluble forms of these proteins. Early studies suggest that the colicin A channel-forming domain undergoes a transition from the native to a molten-globular structure at low pH (12, 13, 15). The molten-globular state is characterized by a preserved secondary structure but a poorly defined tertiary structure, which implies internal segmental dynamics. Our measurement of the NMR chemical shift anisotropies of Cα sites and N–H and C–H dipolar couplings in the colicin Ia channel domain (Huster et al., submitted for publication) supports the preservation of the secondary structure for membrane-bound colicin Ia. Other information on the dynamics of membrane-bound colicins came from recent fluorescence and circular dichroism experiments. These studies found that membrane binding of the colicin E1 channel domain converts the compact helical bundle into a conformationally flexible two-dimensional helical array (16–18) on the surface of the lipid bilayer. This membrane-bound structure is characterized by increased interhelical distances, weaker interhelical interactions, and enhanced motional freedom of the helical segments. Indeed, a proton spin diffusion solid-state NMR study on membrane-bound colicin E1 found that about 60% of the lysine side chains are highly mobile (19). That colicins have pronounced conformational flexibility was also amply demonstrated by conductance measurements of the open channels. For example, experiments using streptavidin binding to immobilize specific biotinylated residues of colicin Ia indicated that during channel opening, a segment of at least 68 residues is

* M.H. thanks the Beckman Foundation for a Beckman Young Investigator Award. D.H. is grateful for a postdoctoral fellowship from the BASF AG and the Studienstiftung des deutschen Volkes.

Corresponding author. E-mail: mhong@iastate.edu, Tel: (515) 294-3521, Fax: (515) 294-0105.

translocated across the membrane (4, 5), and specific portions of the open channel have a dynamic location in the membrane (5, 20).

Solid-state NMR spectroscopy can provide detailed information on the dynamics of insoluble biological macromolecules (1, 21–23). The absence of overall molecular reorientation in the solid state significantly simplifies the analysis of internal segmental dynamics, because the influence of the internal motions on the orientation-dependent spin interactions and nuclear spin relaxation is not obscured by isotropic tumbling of the molecules. The segmental motions can be characterized by order parameters that contain amplitude information and correlation times that provide motional rate information. Both types of parameters can be measured by solid-state NMR with high precision. Motions much faster than the inverse of the anisotropic interaction widths partially average the spectra, from which the segmental order parameters can be derived (24). These order parameters can be interpreted with specific motional models to gain insight into the geometry of the motion (1, 25, 26). The motionally narrowed line shapes also yield the upper limit of the correlation times, although quantitative correlation times for the motion are best obtained from relaxation time constants.

To date, only a few membrane proteins have been characterized dynamically by solid-state NMR (21–23, 27). Large protein systems include bacteriorhodopsin (bR) (28–33), colicin E1 (19), and the coat protein of the filamentous bacteriophage fd (27, 34–36). These solid-state NMR studies indicate that the backbone of membrane-spanning α -helices is essentially rigid, except for a few residues in loop regions and the two termini, while side chains often exhibit discrete jumps between conformational states. In comparison, small membrane peptides are more mobile (23, 37, 38). For instance, gramicidin not only exhibits nanosecond librational motions in the backbone and large-amplitude jump motions in the side chains (8, 9, 39), but also undergoes whole-body rotational diffusion with correlation times of 7 ns parallel and 6 μ s perpendicular to the helix axis (40).

In this work, we employ solid-state NMR spectroscopy to characterize the dynamics of the backbone and side chain segments of the colicin Ia channel domain on the time scales of picoseconds to milliseconds and compare the soluble and membrane-bound states. We show that the membrane-bound state of the colicin Ia channel domain has significantly larger mobility than the soluble state. The motional amplitudes of the backbone and side chains in the soluble protein are limited and are comparable to other crystalline proteins studied so far, but the membrane-bound colicin Ia channel domain acquires dramatically enhanced mobility that distinguishes it from other membrane proteins of comparable size. Our NMR experiments were carried out on uniformly ^{15}N -labeled and selectively and extensively (S&E)¹ ^{13}C -labeled protein samples (41). This special isotopic labeling scheme allowed us to extract the dynamic parameters of the backbones of eight amino acids (Val, Ala, Ser, Gly, Phe, Tyr, Trp, His) and the side chains of two amino acids (Leu and Val) simultaneously. The colicin Ia channel-forming domain consists of 174 amino acids (residues 453–626) (42). It represents one of the largest monomeric membrane proteins whose dynamics have been extensively examined by solid-state NMR.

EXPERIMENTAL PROCEDURES

Materials. 1-Palmitoyl- d_{31} -2-oleoyl-*sn*-glycero-3-phosphocholine (POPC- d_{31}) and 1-palmitoyl-2-oleoyl-*sn*-glycero-3-phosphoglycerol (POPG) were purchased from Avanti Polar Lipids, Inc. (Alabaster, AL), and used without further purification. Colicin Ia channel domain was labeled selectively and extensively in ^{13}C and uniformly in ^{15}N following the TEASE (ten amino acid selective and extensive labeling) labeling protocol (41). ^{15}N -labeled NH₄Cl, ^{15}N -labeled Glu, and 2- ^{13}C -labeled glycerol were purchased from Cambridge Isotopes Laboratories (Andover, MA). Unlabeled amino acids were purchased from Sigma (St. Louis, MO).

Protein Expression. The colicin Ia channel domain was expressed from pKSJ120-containing *E. coli* BL21(DE3) and ^{13}C -labeled by the TEASE protocol published earlier (41). Cells were grown overnight at 37 °C in 100 mL of a modified M9 medium containing, per liter, 1 g of NH₄Cl, 4 g of glycerol, 3 g of KH₂PO₄, 6 g of Na₂HPO₄, 0.5 g of NaCl, 15 mg of CaCl₂, 1 mM MgSO₄, the unlabeled amino acids Asp, Asn, Arg, Gln, Ile, Lys, Met, Pro, Thr, and ^{15}N -Glu at 150 $\mu\text{g}/\text{mL}$ each, and 100 $\mu\text{g}/\text{mL}$ ampicillin. The cells were pelleted and resuspended in 10 mL of the same medium, but containing $^{15}\text{NH}_4\text{Cl}$ and [2- ^{13}C]glycerol. Those cells were used to inoculate 1 L of the stable-isotope-containing medium. The culture was grown at 37 °C to OD₆₆₀ = 0.4 and then induced with 1 mM IPTG. Cells were harvested after 3 h of induction at 37 °C. The soluble His-tagged colicin Ia channel domain was purified on His-Bind metal chelation resin (Novagen, Madison, WI) as specified in the Novagen pET System Manual, except that the wash step was performed at 40 mM imidazole. The yield of the pure soluble protein was approximately 40 mg from 1 L of culture. A comparable amount of protein was unrecoverable from inclusion bodies. Purified protein eluted from the His-Bind resin in 1 M imidazole buffer was dialyzed extensively against distilled water and lyophilized.

Mostly hydrophobic amino acids produced from the glycolysis pathway were ^{13}C -labeled, while the unlabeled amino acids were polar ones produced from the citric acid cycle. Among the ^{13}C -labeled residues, only valine and leucine have directly bonded ^{13}C pairs. By creating many isolated ^{13}C spins and only a small number of directly bonded ^{13}C pairs, the homonuclear ^{13}C – ^{13}C couplings are reduced, which enhances the spectral resolution, and simplifies the assignment of the NMR spectra.

NMR Sample Preparation. For the lipid-free colicin sample, approximately 5.5 mg of protein powder was transferred into a 4 mm magic-angle spinning (MAS) rotor containing a spherical insert. The sample was hydrated with deionized and distilled water to a water content of 30 wt % and sealed.

¹ Abbreviations: bR, bacteriorhodopsin; CODEX, center band only detection of exchange; CP, cross-polarization; CSA, chemical shift anisotropy; CMR7, combined MLEV refocusing and C7; DD, dipolar decoupling; DQF, double quantum filter; PMLG, phase-modulated Lee–Goldburg; MAS, magic-angle spinning; TEASE, ten amino acid selective and extensive labeling; TPPM, two-pulse phase modulation; POPC- d_{31} , 1-palmitoyl- d_{31} -2-oleoyl-*sn*-glycero-3-phosphocholine; POPG, 1-palmitoyl-2-oleoyl-*sn*-glycero-3-phosphoglycerol; rms(d), root-mean-square (deviation); S&E, selective and extensive (labeling); TEDOR, transferred-echo double-resonance; WISE, wide-line separation.

The membrane-bound colicin sample was prepared in the following way. Large unilamellar POPC-*d*₃₁/POPG (3:1, mol/mol) vesicles of a diameter of 100 nm were prepared by extrusion (43) using a hand extruder (Avanti Polar Lipids, Alabaster, AL). Aliquots of extruded lipid vesicles were combined with an appropriate volume of the protein solution to reach a final protein-to-lipid molar ratio of 1:100. The mixture was ultracentrifuged in a swinging-bucket rotor (Beckman Coulter, Inc.) at 150000*g* for 2 h. The aqueous supernatant was analyzed by a photometric assay (44). The analysis revealed that the supernatant contained only about 5% of the initial concentration of the colicin Ia channel domain; thus, 95% of the protein has been reconstituted into the lipid membrane. Since the membrane pellet typically contained 80 wt % water, the pellet was lyophilized and then rehydrated to a final water content of 30 wt % and packed into a 4 mm MAS rotor. The membrane-bound colicin sample contained approximately 8 mg of protein and 24 mg of lipid.

Solid-State NMR Spectroscopy. All NMR experiments were carried out on a Bruker DSX-400 spectrometer (Karlsruhe, Germany) operating at a resonance frequency of 100.72 MHz for ¹³C, 400.49 MHz for ¹H, and 40.59 MHz for ¹⁵N. Either a triple-resonance MAS probe equipped with a 4 mm spinning module or a double-resonance probe with a 5 mm horizontal coil was used. The ¹H radio frequency (rf) field strength for heteronuclear decoupling (45) was about 100 kHz. Carbon and nitrogen 90° pulse lengths were 4.0 and 5.6 μ s, respectively. Cross-polarization (CP) contact time was typically 0.7 ms. Spinning speeds were regulated to \pm 2 Hz by a pneumatic control unit. Recycle delays of 2–3 s were used, and all experiments were carried out at room temperature ($T = 293 \pm 1$ K). Thus, the membrane protein was investigated in the biologically relevant liquid-crystalline phase of the lipid bilayers.

In the following, we briefly describe the pulse sequences of the NMR experiments used in this work.

(A) ¹³C-¹H Coupling Measurement. Figure 1(a) shows the pulse sequence for the double-quantum-filtered (DQF) dipolar and chemical shift (DIPSHIFT) correlation experiment to measure C–H dipolar couplings. It differs from the conventional 2D DIPSHIFT experiment by an additional ¹³C-¹³C double-quantum selection step. The conventional DIPSHIFT experiment measures the C–H dipolar spectra in the indirect dimension and separates them according to the ¹³C isotropic chemical shifts of the various sites in the direct dimension (46). For the membrane-bound colicin Ia channel protein, this experiment will detect the ¹³C signals of the lipid carbons as well as the protein carbons, and partial overlap of the two will bias the measurement of the C–H couplings of the protein. The DQF-DIPSHIFT experiment solves this problem by suppressing the single-quantum ¹³C coherences from isolated spins, which include the lipid carbons, and detecting only ¹³C spin pairs. With the TEASE ¹³C labeling strategy, the Val C α and C β sites and the Leu C β and C γ sites were selected. It is fortunate that the strongest lipid signal, the (CH₂)_n peak, overlaps with the Val C β signal, which is selected by the DQF-DIPSHIFT experiment, while most other protein resonances are free of any significant lipid background signals, and thus can be measured using the simple DIPSHIFT experiment.

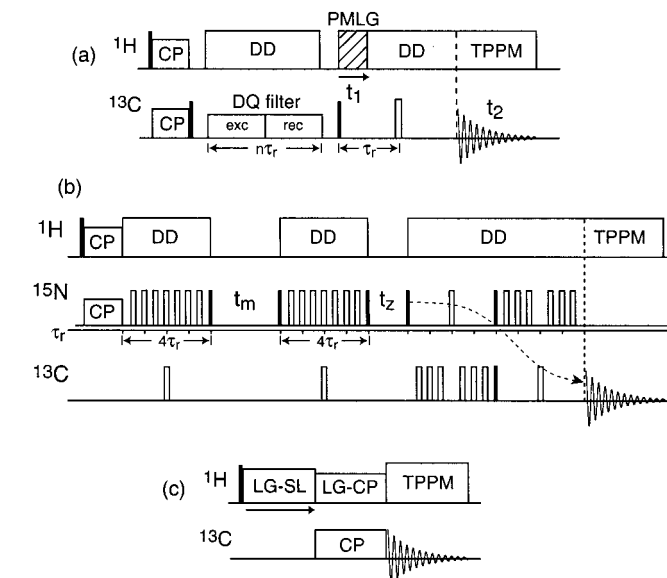


FIGURE 1: Pulse sequences used in this work to characterize colicin dynamics. (a) 2D double-quantum-filtered dipolar chemical shift (DQF-DIPSHIFT) correlation experiment, for measuring C–H dipolar couplings of protein ¹³C signals that overlap with the lipid signals. A double-quantum filter (exc, excitation; rec, reconversion) precedes the C–H dipolar evolution period, t_1 , during which ¹H homonuclear decoupling is achieved with the PMLG sequence. (b) ¹³C-detected ¹⁵N CODEX experiment for detecting millisecond time scale motions. Segmental reorientations during the mixing time, t_m , were detected through changes in the ¹⁵N chemical shift anisotropy. ¹³C detection enhances the sensitivity and resolution of the spectra. (c) ¹H $T_{1\rho}$ experiment for investigating microsecond time scale motions. Lee–Goldburg spin-lock (LG-SL) and Lee–Goldburg cross-polarization (LG-CP) are used to achieve site specificity. Filled and open rectangles represent 90° and 180° pulses, respectively. Continuous-wave dipolar decoupling (DD) of the protons was used in the experiments, except for the acquisition period, when two-pulse phase-modulation (TPPM) was applied.

Double-quantum filtration was accomplished by applying the CMR7 homonuclear dipolar recoupling sequence (47) before the C–H evolution period. At the spinning speed of $\omega_r/2\pi = 7000$ Hz, a ¹³C rf field strength of 49 kHz was required for CMR7 recoupling during the double-quantum excitation and reconversion periods.

In the C–H coupling experiments, ¹H–¹H homonuclear decoupling was accomplished using either the MREV-8 sequence (48) at a spinning speed of $\omega_r/2\pi = 4252$ Hz or the phase-modulated Lee–Goldburg (PMLG) sequence (49, 50) at a spinning speed of $\omega_r/2\pi = 7000$ Hz or higher. In the MREV-8 sequence, the 90° pulse was 2.8 μ s, and seven semi-windowless MREV-8 cycles were matched to one rotor period. At the faster spinning speeds of 7000 and 9333 Hz, PMLG decoupling was achieved by a linear phase ramp during each 360° pulse (50). The amplitude of the phase modulation was 208° to meet the Lee–Goldburg condition, since $208^\circ/360^\circ = \phi_{\text{PMLG}}/\phi_{\text{eff}} = \omega_{\text{PMLG}}/\omega_{\text{eff}} = \cos(54.7^\circ)$. Here ω_{PMLG} is the frequency offset, and ω_{eff} is the effective field strength, and ϕ_{PMLG} and ϕ_{eff} represent the respective phase angles.

We conducted the C–H DIPSHIFT experiments in a constant-time fashion, so that the time signals of only one rotor period were acquired in the t_1 dimension. Since the dipolar-induced signal decay is periodic with the rotor period, the constant-time evolution yields the same dipolar coupling information as a normally incremented 2D experiment (51,

52). The one-rotor-period time domain data were fit to yield the coupling strength of interest. This analysis of the time domain data of the indirect dimension (t_1) yields the same information as the spinning-sideband analysis in the frequency domain (ω_1).

(B) ^1H - ^1H Coupling Measurement. ^1H - ^1H dipolar couplings were measured using the ^1H wide-line separation (WISE) experiment at $\omega_r/2\pi = 7000$ Hz (53). A short CP contact time of 100 μs was used to minimize the effects of ^1H spin diffusion. The widths of the WISE spectra were obtained from the full width at half-height of the intensity envelop of the spinning sideband patterns.

(C) ^{15}N Exchange Measurement. To investigate slow motions in the 10^{-3} –1 s time window, we conducted the ^{13}C -detected ^{15}N CODEX (centerband only detection of exchange) experiment under MAS (54, 55). The pulse sequence is shown in Figure 1(b). ^{15}N magnetization, created by ^1H - ^{15}N cross-polarization, evolves under the recoupled chemical shift anisotropy (CSA) interaction for four rotor periods before and after a mixing period t_m . During these periods, orientation-dependent ^{15}N CSA phases Φ_1 and Φ_2 were acquired. The ^{15}N CSA interaction was recoupled by 180° pulses spaced half a rotor period apart, while the 180° ^{13}C pulses refocus the undesired ^{13}C - ^{15}N dipolar coupling. A pair of ^{15}N 90° pulses flanking the mixing period selects ^{15}N magnetization terms that are modulated by $\cos \Phi_1 \cos \Phi_2$ and $\sin \Phi_1 \sin \Phi_2$ in two consecutive scans. Addition of the two scans yields magnetization of the type $N_x [\cos(\Phi_1 - \Phi_2)]$. If motion is absent during t_m , then $\cos(\Phi_1 - \Phi_2) = 1$, and the magnetization is completely refocused. If segmental reorientation occurs on the millisecond time scale (but not on the microsecond time scale), then a reduced ^{15}N signal is observed due to $\cos(\Phi_1 - \Phi_2) < 1$. Thus, segmental reorientation is manifested as intensity changes between a control experiment with $t_m = 0$ and an exchange experiment with a finite t_m . The exchange is detected through ^{13}C spectra by transferring ^{15}N magnetization to ^{13}C using a transferred-echo double-resonance (TEDOR) pulse sequence (56). The ^{15}N spins are good probes of molecular dynamics since they are not prone to spin diffusion and the amide ^{15}N CSAs are sufficiently large to be sensitive to small-angle reorientations.

The ^{13}C -detected ^{15}N CODEX experiments were carried out at a spinning speed of $\omega_r/2\pi = 11$ kHz at mixing times of 1, 100, 250, and 400 ms. The z-filter time, t_z , was 1 ms. Ramp CP (57) from ^1H to ^{15}N was used with a contact time of 1 ms. For the control experiments, t_m and t_z were reversed, so that the contributions of T_1 relaxation to signal losses were equalized between the control and exchange experiments.

(D) $^1\text{H} T_{1\rho}$ Measurement. The ^1H rotating-frame relaxation time constants were measured using the pulse sequence of Figure 1(c). ^1H magnetization, created by a 54.7° (magic-angle) pulse, was locked by a Lee–Goldburg (LG) spin-lock sequence (58) for a variable delay. During the spin-lock period, the ^1H - ^1H dipolar interaction was decoupled to abolish spin diffusion. The ^1H magnetization was then transferred to ^{13}C by a Lee–Goldburg CP step and detected. This spin-diffusion-free experiment allows $^1\text{H} T_{1\rho}$ to be measured site-specifically. The experiment was performed at a spinning speed of $\omega_r/2\pi = 7$ kHz. Effective ^1H field strengths of $\gamma B_{\text{eff}}/2\pi = 55, 70$, and 85 kHz and variable delays between 1 and 17 ms were used for the LG spin-lock. The LG-CP contact time was 300 μs . $T_{1\rho}$ values were

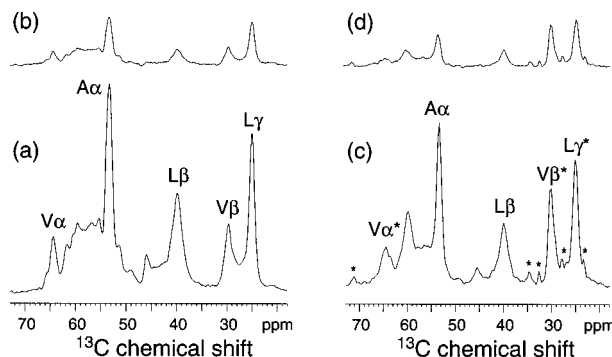


FIGURE 2: ^{13}C cross sections of the 2D ^{13}C - ^1H DIPSHIFT spectra, extracted at dipolar evolution times of $t_1 = 0$ (a, c) and $t_1 = \tau_r/2$ (b, d). The spectra of both the soluble (a–b) and the membrane-bound (c–d) colicin Ia channel domain are shown. Asterisks indicate lipid background signals. The spectra were acquired at a spinning speed of $\omega_r/2\pi = 7$ kHz, corresponding to $\tau_r = 142.9 \mu\text{s}$. Dipolar dephasing was observed over 1 rotor period sampling 17 data points, including the rotor echo. Typically, 640 and 1280 transients were accumulated per t_1 slice at a recycle delay of 3 s, yielding total acquisition times of about 9 and 18 h for the soluble and membrane-bound samples, respectively.

extracted as the decay constant of the single exponential that best-fits the experimental intensities as a function of the spin-lock delays.

(E) ^{15}N Chemical Shift Anisotropy Measurement. Static ^{15}N spectra were acquired with a standard CP pulse sequence with Hahn echo detection. A ^1H - ^{15}N CP contact time of 1 ms was used.

Simulations. The time evolution under the C–H dipolar couplings was simulated for one rotor period using a Fortran program described before (52). Simulations were carried out for varying CH dipolar coupling strengths. Powder averaging was performed in 3° increments for all three Euler angles. Further input parameters are sample spinning speed and the number of time domain points. All simulations were performed on a Macintosh G4 computer. The simulated curves were multiplied with an exponential decay to account for T_2 relaxation effects during the dipolar evolution. Best agreement between simulation and experiment was determined by the smallest rmsd values.

RESULTS

C–H and H–H Couplings. We measured the ^{13}C - ^1H and ^1H - ^1H dipolar couplings in colicin to investigate motions on the sub-microsecond time scale. These motions may include protein peptide plane librations and discrete side chain jumps with rates greater than the static interaction strength. The ratio of the motionally reduced coupling strength ($\bar{\delta}$), averaged over all possible tensor orientations sampled on the NMR time scale, and the rigid-limit coupling (δ) defines the segmental order parameter $S = \bar{\delta}/\delta$, which contains valuable information on the motional amplitude (59, 60).

We measured the C–H dipolar couplings for the soluble and membrane-bound colicin Ia channel domain using the DIPSHIFT and DQF-DIPSHIFT experiments. The theoretical value for the rigid-limit one-bond ^{13}C - ^1H dipolar coupling is ~ 23 kHz. This defines an upper limit of $\sim 40 \mu\text{s}$ for the motional correlation times that the experiment is sensitive to. Figure 2 shows several ω_2 slices, corresponding to the

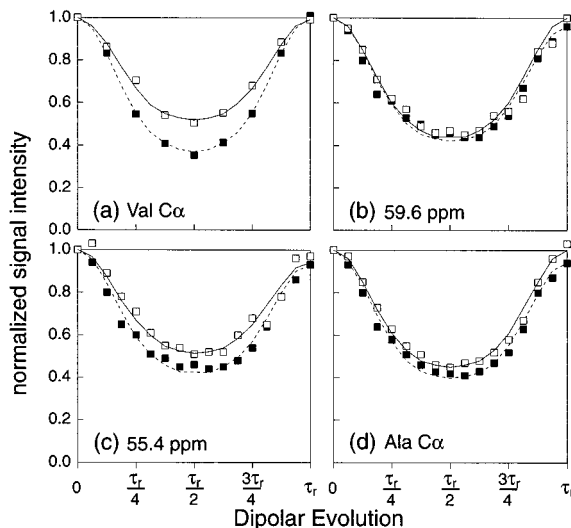


FIGURE 3: C–H dipolar dephasing curves for backbone sites of the soluble (filled symbols) and membrane-bound colicin (open symbols), extracted from 2D datasets of the type (t_1, ω_2). Cross sections at ^{13}C isotropic shifts of 64.4 ppm for Val C α (a), 59.6 ppm (b), 55.4 ppm (c), and 53.2 ppm for Ala C α (d) are shown. Dashed and solid lines represent best fits for the soluble and membrane-bound colicin signals, respectively. The resulting coupling strengths are given in Table 2. Panel (a): Val C α was obtained from a DQF-DIPSHIFT experiment to eliminate lipid background signals. For the DQF-DIPSHIFT experiment, 9 data points were sampled in t_1 , with 2240 and 3072 scans per increment for the soluble and the membrane samples, respectively, yielding acquisition times of 14 and 19 h. The other panels show data obtained from the conventional DIPSHIFT experiment with the same conditions as in the Figure 2 caption.

^{13}C isotropic chemical shift dimension, of the 2D DIPSHIFT spectra for the soluble [(a), (b)] and membrane-bound colicin [(c), (d)] at different dipolar evolution times. At $t_1 = 0$, the ^{13}C slices are equivalent to the CP spectra [Figure 2(a),(c)]. Partial peak assignment is given in Figure 2(a) based on experiments described in a separate paper. Peaks marked with an asterisk represent either lipid resonances or protein signals that overlap with lipid background signals. After a dipolar evolution time of $\tau_r/2$, the intensities of both samples were significantly reduced due to dephasing under the C–H dipolar couplings [Figure 2(b),(d)]. The ^{13}C – ^1H dipolar dephasing curves over one rotor period for several backbone and side chain segments are shown in Figures 3 and 4, respectively. Note that these were extracted from 2D data sets (t_1, ω_2) that have been Fourier-transformed only in the direct dimension. The time signals of the soluble protein are represented by filled symbols and the membrane-bound protein by open symbols. In all cases, smaller dephasing was observed for the membrane-bound protein, indicating smaller ^{13}C – ^1H dipolar couplings. Since the Val C α signal of the membrane-bound sample overlaps with a weak lipid glycerol signal, the DQF-DIPSHIFT experiment was used to obtain the Val C α dephasing curve [Figure 3(a)]. The coupling strengths, obtained from the best fits to the experimental decay curve, are listed in Table 1. Scaling these coupling strengths with the rigid-limit value yielded the order parameters S_{CH} for both states of the protein (Table 1). To take into account the effects of nonideal scaling factors of the homonuclear decoupling sequences, we directly measured the rigid-limit coupling strengths for CH and CH₂ groups from the C α sites of polycrystalline leucine and glycine,

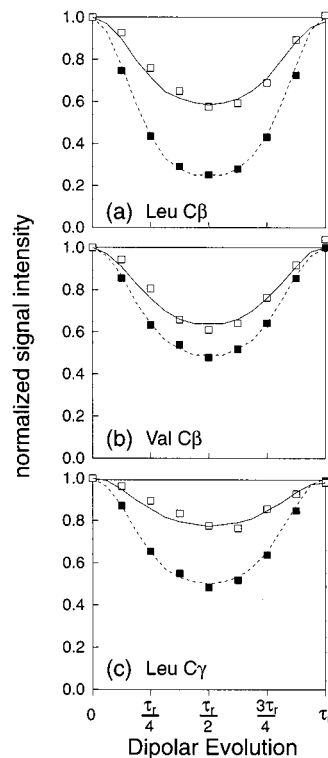


FIGURE 4: C–H dipolar dephasing curves for colicin side chain segments, extracted from DQF-DIPSHIFT spectra. (a) Leu C β , (b) Val C β , (c) Leu C γ . Both soluble (filled symbols) and membrane-bound colicin (open symbols) are shown, with the respective best fits shown as dashed and solid lines (Table 1).

Table 1: C–H Dipolar Coupling Strengths ($\bar{\delta}_{\text{CH}}$) and Order Parameters (S_{CH}) for Various Sites of the Colicin Ia Channel Domain in the Soluble and Membrane-Bound Forms

^{13}C chemical shift (ppm)	soluble colicin		membrane-bound colicin	
	$\bar{\delta}_{\text{CH}}$	S_{CH}^a	$\bar{\delta}_{\text{CH}}$	S_{CH}^a
64.4 (Val α)	12.7 ^b	1.00 ± 0.05^d	10.6 ^b	0.90 ± 0.02^d
59.6	11.9 ^c	0.95 ± 0.04^e	11.8 ^c	0.90 ± 0.03^e
56.8	12.1 ^c	0.96 ± 0.04^e	10.8 ^c	0.88 ± 0.04^e
55.4	12.1 ^c	0.97 ± 0.03^e	11.3 ^c	0.90 ± 0.02^e
53.2 (Ala α)	12.3 ^c	0.97 ± 0.03^e	11.6 ^c	0.93 ± 0.03^e
39.7 (Leu β)	14.4 ^c	0.88 ± 0.02^e	10.8 ^c	0.66 ± 0.05^e
29.6 (Val β)	11.1 ^b	0.88 ± 0.05^d	8.9 ^b	0.75 ± 0.02^d
24.9 (Leu γ)	10.9 ^b	0.87 ± 0.05^d	6.6 ^b	0.60 ± 0.03^d

^a Order parameters are calculated by dividing the measured dipolar couplings by the values measured for the rigid crystalline amino acids Leu C α (CH) and Gly C α (CH₂). The measured rigid-limit coupling strengths are: $\delta_{\text{CH}} = 11.5$ kHz under MREV-8 decoupling, $\delta_{\text{CH}} = 12.8$ kHz under PMLG decoupling, and $\delta_{\text{CH}_2} = 16.3$ kHz under PMLG decoupling. In the DQF-DIPSHIFT experiment, a slightly smaller $\delta_{\text{CH}} = 11.9$ kHz was found under PMLG decoupling. ^b DQF-DIPSHIFT experiment (7 kHz spinning speed with PMLG decoupling). ^c Conventional DIPSHIFT experiment (7 kHz spinning speed with PMLG decoupling). ^d Random experimental error from two different experiments. ^e Average of four DIPSHIFT experiments at spinning speeds of 4252 Hz (MREV-8 decoupling), 7000 Hz, and 9333 Hz (both PMLG decoupling); error limit represents standard deviation.

respectively. We found that the backbone S_{CH} values fall within the range of 0.95–1.00 for the soluble state but are reduced to 0.88–0.93 for the membrane-bound protein. Thus, the reduction factor from the soluble state to the membrane-bound state is about 0.9.

Even larger reductions of the C–H couplings were found for the side chains upon membrane binding. Figure 4 shows the dipolar dephasing curves for Leu C β (a), Val C β (b),

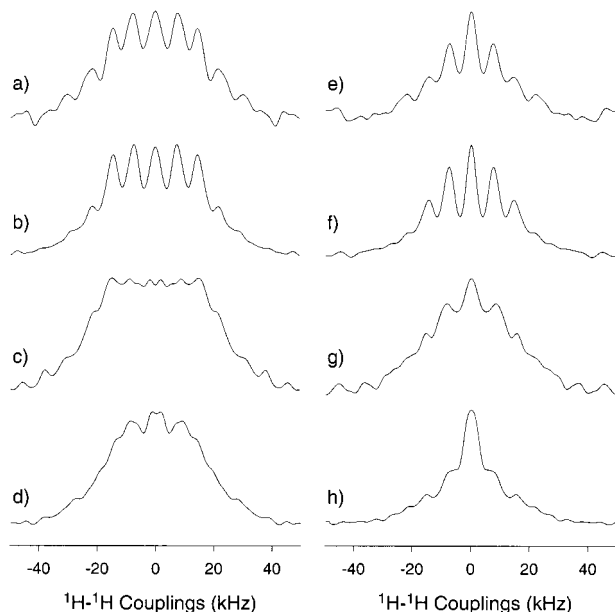


FIGURE 5: ¹H cross sections of the 2D WISE spectra of soluble (a–d) and membrane-bound colicin (e–h), extracted at ¹³C isotropic shifts of (a, e) 59.6 ppm, (b, f) 53.2 ppm for Ala C α , (c, g) 39.7 ppm for Leu C β , and (d, h) 24.9 ppm for Leu C γ . The estimated coupling strengths are given in Table 2. The spectra were acquired at $\omega_r/2\pi = 7$ kHz and with a total ¹H evolution time of 0.5 ms. A total of 128 and 224 transients were acquired for each t_1 slice for the soluble and membrane-bound sample, respectively, yielding acquisition times of 4 and 8 h.

and Leu C γ (c) for both states of the protein. Since both the Val C β and Leu C γ resonances overlap with lipid signals, the DQF-DIPSHIFT experiment was used to acquire these data. The best fits to the experimental data yielded side chain S_{CH} values of approximately 0.87–0.88 for the soluble colicin, but smaller S_{CH} 's of 0.60–0.75 for the membrane-bound colicin Ia channel domain (Table 1). The average reduction factor from the soluble to the membrane-bound protein is about 0.69–0.85.

The motional narrowing induced by membrane binding was confirmed by the ¹H-¹H dipolar couplings, which were measured using the WISE experiment. The ¹H-¹H dipolar couplings in typical organic solids are on the order of 40–50 kHz; thus, they are sensitive to motions with correlation times of less than 20 μ s. Figure 5 shows cross sections of the WISE spectra of the soluble (left column) and membrane-bound (right column) colicin Ia channel domain at various sites. The broadest spectra have homogeneous line widths of about 50 kHz. While the line shapes are complex due to the ¹H multi-spin system, it is evident that the spectra of all sites are much narrower for the membrane-bound protein than for the soluble protein. Using the full width at half-maximum of the spinning sideband intensity envelope as the criterion, we estimated the coupling strengths of these two protein samples (Table 2). The ratio, K_{HH} , of the couplings between the soluble and the membrane-bound proteins represents the additional motions induced by membrane binding. These motional narrowing factors range from 0.29 for the side chain Val C β to 0.67 for the backbone C α of Ala (Table 2).

¹⁵N Chemical Shift Anisotropy. The line shape of static ¹⁵N chemical shift spectra can also be used to determine the presence or absence of motions. The rigid-limit ¹⁵N chemical

Table 2: H–H Dipolar Coupling Strengths for Various Sites of the Colicin Ia Channel Domain in the Soluble ($\bar{\delta}_{CH,sol}$) and Membrane-Bound ($\bar{\delta}_{CH,MB}$) Forms

¹³ C chemical shift (ppm)	$\bar{\delta}_{HH,sol}$ (kHz), soluble colicin	$\bar{\delta}_{HH,MB}$ (kHz), membrane-bound colicin	$K_{HH} = \bar{\delta}_{HH,MB}/\bar{\delta}_{HH,sol}$
64.4 (Val α)	35.0	15.0	0.43
59.6	42.8	26.7	0.62
56.8	39.0	19.0	0.49
55.4	40.0	21.3	0.53
53.2 (Ala α)	42.5	28.8	0.67
39.7 (Leu β)	51.3	31.3	0.61
29.6 (Val β)	42.5	12.5	0.29
24.9 (Leu γ)	38.8	15.0	0.39

shift anisotropy of backbone amides in proteins is typically $\Delta\sigma \approx 160$ ppm with an asymmetry parameter of $\eta \approx 0.15$ (61). At the ¹⁵N Larmor frequency of 40.59 MHz used here, this anisotropic interaction makes the ¹⁵N spectra sensitive to motions with correlation times shorter than 150 μ s. The ¹⁵N CSA is primarily sensitive to backbone motions, such as peptide plane librations and small-amplitude reorientations of entire helices. Figure 6 shows the static ¹⁵N spectra of the soluble (solid line) and membrane-bound colicin (dashed line). Considering that both spectra represent the superposition of many residues, the powder line shapes are quite similar to a single chemical shift pattern of approximate axial symmetry. The spectrum of the soluble protein has a width of about 163 ppm, while the membrane-bound protein exhibits a width of 156 ppm, a 5% reduction. This suggests that membrane binding induces small-amplitude motions. In addition to the slight reduction in the CSA, a small hump at about 120 ppm in the spectrum of the membrane protein is detected. We speculate that it may originate from downfield-shifted 90° edges of a subset of powder patterns with motionally reduced anisotropies. Thus, a small fraction of residues in the membrane-bound protein may undergo larger-amplitude motions than the rest.

¹⁵N Exchange under MAS. We further investigated whether slow motions on the millisecond to second time scales exist in colicin Ia channel domain in either conformation. To probe motions in this time window, we carried out the ¹³C-detected ¹⁵N CODEX experiment. Figure 7 shows the C α region of the CODEX exchange spectra of soluble (a) and membrane-bound (c) protein acquired with a mixing time of 400 ms. The corresponding control spectra are given in Figure 7 (b), (d), respectively. Within experimental sensitivities, no differences between the exchange and the control spectra were detected, indicating that no reorientational motions occur within 400 ms in either the soluble or the membrane-bound state of the colicin Ia channel domain.

Proton $T_{1\rho}$. While the above experiments examine the motional amplitudes and their effects on the spectral line shapes, relaxation time constants yield information on the motional rates. Rotating-frame spin–lattice relaxation times are sensitive to molecular motions on the 10⁻⁶ s time scale, or the inverse of the spin-lock field strength (62). These may include small-angle reorientations of entire secondary structure elements (63). We measured the ¹H $T_{1\rho}$ relaxation times in the colicin Ia channel domain using a Lee–Goldburg spin-lock experiment. This allowed us to obtain the true relaxation times without interference from ¹H spin diffusion, and to assign these relaxation times to spectrally resolved segments

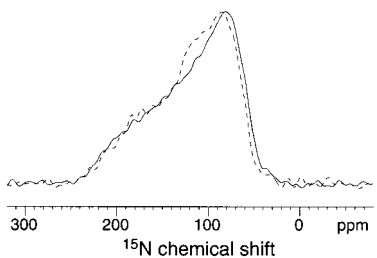


FIGURE 6: ^{15}N static powder spectra for soluble (solid line) and membrane-bound colicin (dashed line). A total of 21 552 and 26 528 scans were coadded at a recycle delay of 2 s for the soluble and membrane-bound protein, respectively.

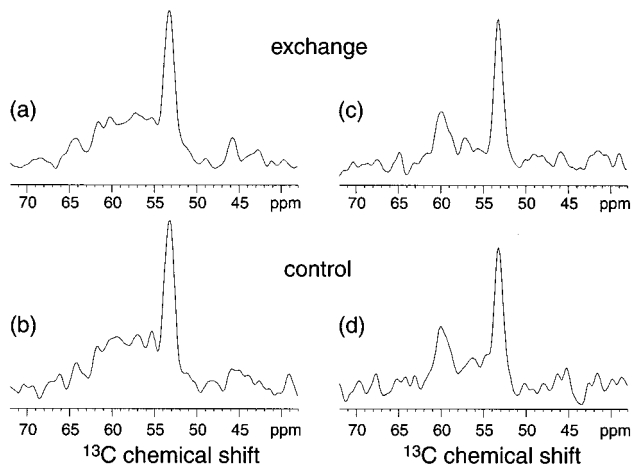


FIGURE 7: ^{13}C -detected ^{15}N CODEX spectra for the soluble (a–b) and the membrane-bound (c–d) colicin Ia channel domain. A mixing time of 400 ms and a spinning speed of $\omega_r/2\pi = 11$ kHz were used. (b, d) Control spectra. (a, c) Exchange spectra. The control spectra were acquired with a z-filter (t_2) of 400 ms and a mixing time of 1 ms. A total of 2048 (a), 1024 (b), 6144 (c), and 3072 (d) scans were coadded at a recycle delay of 2.1 s.

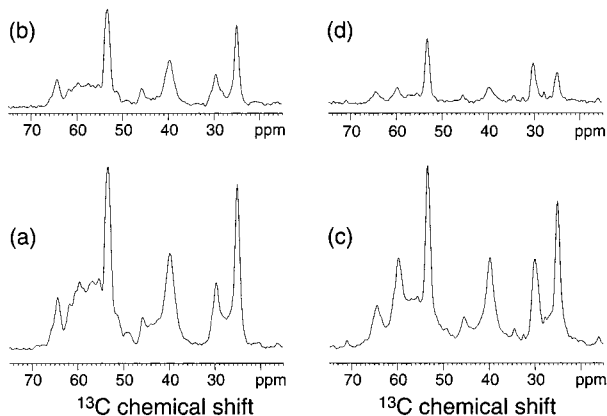


FIGURE 8: 1D ^{13}C spectra of the soluble (a–b) and the membrane-bound (c–d) colicin Ia channel domain after ^1H spin-lock delays of 1 μs (a, c) and 10 ms (b, d). A ^1H spin-lock field of 85 kHz and a spinning speed of 7 kHz were used. A total of 368 and 800 transients were added for the soluble and membrane-bound sample, respectively. Spectra (a) and (c) were scaled to the same maximum intensity to illustrate the faster intensity decay for the membrane-bound sample.

in the protein.

Figure 8 shows the ^{13}C spectra acquired with a ^1H spin-lock field strength of 85 kHz and delays of 1 μs [(a), (c)] and 10 ms [(b), (d)] for the soluble (left column) and the membrane-bound colicin (right column). Spectra (a) and (c) were scaled according to the intensity of the 53.2 ppm peak.

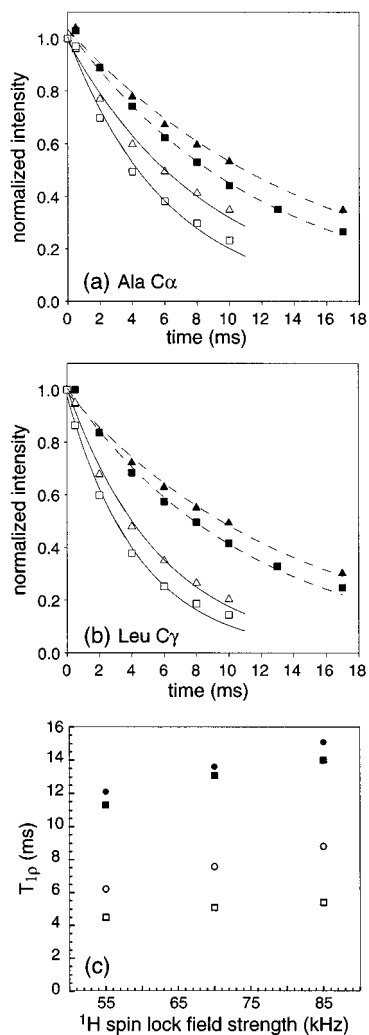


FIGURE 9: ^1H rotating-frame relaxation times, $T_{1\rho}$, of the colicin Ia channel domain. (a–b) ^{13}C intensities as a function of the spin-lock delay. (a) Backbone Ala C α . (b) Side chain Leu C γ . Soluble colicin: filled symbols. Membrane-bound colicin: open symbols. Data were acquired at spin-lock field strengths of 55 kHz (squares) and 85 kHz (triangles). Dashed and solid lines represent best-fit single-exponentials for the soluble and membrane-bound protein, respectively. (c) ^1H $T_{1\rho}$ as a function of the spin-lock field strengths for Ala C α (circles) and Leu C γ (squares).

It is seen that the membrane-bound colicin exhibits larger intensity reduction with time, indicating shorter proton $T_{1\rho}$'s. To extract quantitative $T_{1\rho}$ values, the intensity decays as a function of the spin-lock time were fit to single-exponential functions. Representative decay curves of the backbone and side chain segments were shown for the Ala C α [Figure 9(a)] and the Leu C γ [Figure 9(b)] peaks, respectively. The trend of faster decays for the membrane-bound protein was general, and was maintained at weaker spin-lock field strengths. The extracted decay constants, $T_{1\rho}$, at three spin-lock fields (85, 70, and 55 kHz) and for various sites are listed in Table 3. The $T_{1\rho}$ values for the Ala C α and Leu C γ sites as a function of the field strengths are also displayed in Figure 9(c). We found that the $T_{1\rho}$ values of the membrane-bound protein are shorter by a factor of 2–3 compared to the soluble protein. Further, the $T_{1\rho}$ values vary with the spin-lock field strength in both forms of the colicin Ia channel domain. This suggests that the correlation times are either near the minimum or on the slow side of the minimum of the logarithmic $T_{1\rho}$ – τ plot.

Table 3: Proton $T_{1\rho}$ Values and Effective Correlation Times (τ_e) for the Soluble and Membrane-Bound Colicin Ia Channel Domains at Three Different Spin-Lock Field Strengths

^{13}C chemical shift (ppm)	soluble colicin				membrane-bound colicin			
	$T_{1\rho}$ (ms)			τ_e (μs)	$T_{1\rho}$ (ms)			τ_e (μs)
	55 kHz	70 kHz	85 kHz		55 kHz	70 kHz	85 kHz	
64.4 (Val α)	12.4	13.3	15.4	0.9	4.9	6.1	6.7	1.2
59.6	7.8	8.2	9.4	0.8	3.6	4.4	4.9	1.2
56.8	7.2	7.4	8.4	0.6	2.8	3.4	4.2	1.6
53.2 (Ala α)	12.1	13.6	15.1	0.9	6.2	7.6	8.8	1.3
39.7 (Leu β)	11.4	13.1	13.4	0.7	3.7	4.5	5.0	1.1
24.9 (Leu γ)	11.3	13.1	14.0	0.8	4.5	5.1	5.4	0.8

To extract the motional correlation times, we consider the $T_{1\rho}$ relaxation to be driven by $^1\text{H}-^1\text{H}$ dipolar couplings and the one-bond $^1\text{H}-^{13}\text{C}$ dipolar couplings. The small proton CSAs can be neglected as a relaxation mechanism. The powder-averaged ^1H rotating-frame relaxation rate can then be written as (59)

$$\frac{1}{T_{1\rho}} = \frac{3}{2} \delta_{\text{HH}}^2 \{ 3 \sin^2 \beta \cos^2 \beta J(\omega_e) + 3 \sin^4 \beta J(2\omega_e) + (5 - 3 \cos^2 \beta) J(\omega_H) + (6 \cos^2 \beta + 2) J(2\omega_H) \} + \frac{3}{2} \delta_{\text{CH}}^2 \left\{ \sin^2 \beta \left[\frac{2}{3} J(\omega_e) + J(\omega_C) \right] + (1 + \cos^2 \beta) \left[\frac{1}{6} J(\omega_C - \omega_H) + \frac{1}{2} J(\omega_H) + J(\omega_C + \omega_H) \right] \right\} \quad (1)$$

Here, $\delta_{\text{CH}} = (\mu_0/4\pi)\gamma_H\gamma_C\hbar/r_{\text{CH}}^3$ and $\delta_{\text{HH}} = (\mu_0/4\pi)\gamma_H^2\hbar/r_{\text{HH}}^3$ are the rigid-limit dipolar coupling strengths, μ_0 is the permeability of free space, γ_H and γ_C are the gyromagnetic ratios of ^1H and ^{13}C , $2\pi\hbar$ is the Planck constant, and $r_{\text{CH}} = 1.1 \text{ \AA}$ is the C–H bond length. The angle β between the external magnetic field and the effective field of the spin-lock pulse is 54.7° . The spectral density functions $J(\omega_i)$ are evaluated at the sum and difference frequencies of the effective field strength ω_e of the spin-lock pulse, the ^1H Larmor frequency ω_H , and the ^{13}C Larmor frequency ω_C . We assume that a single motional mechanism describes the segmental reorientations; then the spectral density function is given by (64, 65)

$$J(\omega_i) = (1 - S^2) \frac{\tau}{1 + \omega_i^2 \tau^2} \quad (2)$$

where S is the generalized order parameter of the motion and τ is the correlation time. Substituting $\beta = 54.7^\circ$ into eq 1, we obtain a simpler expression for $T_{1\rho}$:

$$\frac{1}{T_{1\rho}} = \frac{1}{10} \delta_{\text{HH}}^2 \{ J(\omega_e) + 2J(2\omega_e) + 6J(\omega_H) + 6J(2\omega_H) \} + \frac{1}{30} \delta_{\text{CH}}^2 \{ 2J(\omega_e) + 3J(\omega_C) + J(\omega_C - \omega_H) + 3J(\omega_H) + 6J(\omega_C + \omega_H) \} \quad (3)$$

Two more parameters need to be considered before the correlation time τ can be extracted from $T_{1\rho}$. First, the H–H coupling δ_{HH} does not have a well-defined value due to the complex multispin system of protons. But the ^1H WISE spectra shown above yielded average couplings of 40 kHz for C–H groups in the relatively rigid soluble colicin (Table 2). Thus, we used $\delta_{\text{HH}} = 40 \text{ kHz}$ in our calculations. Second,

the generalized order parameter, S , usually differs from S_{CH} obtained from line shape experiments except for axially symmetric motions (64). In addition, the generalized C–H and H–H order parameters suitable for eq 3 can be different. To simplify the calculations, we assume that a single generalized order parameter can be used to describe the motion of each aliphatic segment. This allows us to use the ratio of two $T_{1\rho}$ values at two different spin-lock field strengths to extract the correlation times. This procedure reduces the effects of the uncertainties in the order parameters as well as in δ_{HH} on the correlation time determination. Figure 10 shows a semilog plot of the $T_{1\rho}$ ratio between $\omega_e = 85 \text{ kHz}$ and $\omega_e = 55 \text{ kHz}$ as a function of the correlation time τ for several δ_{HH} . At $\omega_e\tau \ll 1$, a constant $T_{1\rho}$ ratio of 1 was obtained, corresponding to the fast side of the standard logarithmic $T_{1\rho}-\tau$ plot. At $\omega_e\tau \gg 1$, the $T_{1\rho}$ ratio reaches a maximum of about 2.4. When $\omega_e\tau \approx 1$, which corresponds to correlation times of $1-3 \mu\text{s}$ for the spin-lock field strengths used here, the $T_{1\rho}$ ratio depends most sensitively on τ . Averaging the three experimental $T_{1\rho}$ ratios at the different field strengths, we obtained correlation times of about $0.8 \mu\text{s}$ for the segments in the soluble colicin and about $1.2 \mu\text{s}$ for the membrane-bound colicin Ia channel domain (Table 3). The ranges of the $T_{1\rho}$ values for various residues in the two states of the protein are shown as shaded areas in Figure 10. The extracted correlation times are quite insensitive to the value of δ_{HH} used: an uncertainty in δ_{HH} of $\pm 10 \text{ kHz}$ translates to less than 5% uncertainty in τ obtained in this way.

DISCUSSION

Our motivation for the current study is to understand how environmental factors influence the molecular dynamics of the colicin Ia channel domain, and how such motions may facilitate the function of the protein as a bacteriocin. The broader motivation is to use colicin as a model system to gain insights into membrane protein dynamics and its relation to function. Previous studies suggest that membrane protein dynamics are a complex process that is related to the specific function of the individual proteins (4, 5, 8–10). Both bacteriorhodopsin and the fd coat protein have been found to be mostly rigid. In contrast, the colicin Ia channel domain, examined here in two different states, water-soluble and membrane-bound, on a range of time scales, and through a number of nuclear spin interactions, emerges as an initially rigid molecule whose conformational flexibility is greatly amplified by binding to the lipid bilayer.

Sub-microsecond Colicin Dynamics. We have measured the motionally narrowed C–H and H–H dipolar spectra and ^{15}N CSA to obtain information on the motional amplitudes

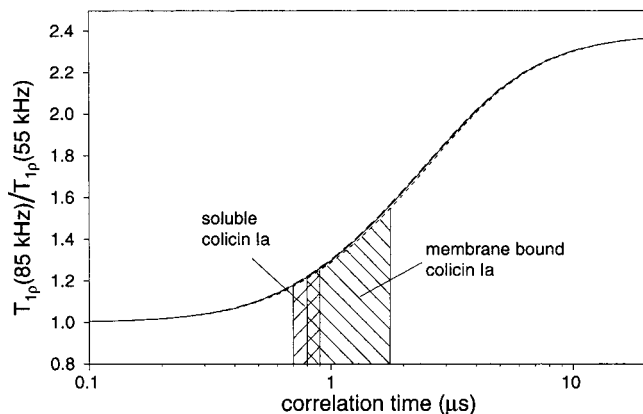


FIGURE 10: Dependence of ^1H $T_{1\rho}$ on the motional correlation time τ (lines) and the distribution of τ for the soluble and membrane-bound colicin Ia channel domain. $T_{1\rho}$ ratios for spin-lock field strengths of 85 and 55 kHz were calculated using eqs 2 and 3. Three ^1H - ^1H dipolar couplings of 30 kHz (dotted line), 40 kHz (solid line), and 50 kHz (dashed line) were considered. They show negligible effects on the extraction of the correlation times.

of the colicin Ia channel domain. Segmental motions with correlation times shorter than about 10^{-5} s were probed by these experiments. Membrane binding reduces the couplings in both the backbone and the side chains, but to different extents.

(A) *Backbone Motions.* Both the soluble and membrane-bound states of the colicin Ia channel domain exhibit reduced C–H dipolar couplings compared to rigid molecules. C–H order parameters of 0.95 or higher were obtained for the soluble colicin, while an average value of 0.9 was measured for the membrane-bound protein (Table 1). In the limit of small amplitudes for the motion, the root-mean-square (rms) angular fluctuations, $\sqrt{\langle \theta^2 \rangle}$, can be extracted from the definition of the order parameter for axially symmetric motions according to (64)

$$S = 1 - \frac{3}{2} \langle \theta^2 \rangle \quad (4)$$

For the soluble colicin, $S_{\text{CH}} = 0.95–1.00$ correspond to rms amplitudes of $10–0^\circ$. Such small-amplitude motions are usually attributed to backbone librations on the sub-nanosecond time scale based on relaxation studies and ^2H NMR. Interestingly, the order parameters for colicin Ia appear slightly larger than what are typically measured for globular proteins in solution ($S \sim 0.93$) (1) and for the crystalline staphylococcal nuclease (65) or lysozyme (66). This resulted from the fact that we used the experimentally measured couplings in crystalline amino acids as the rigid-limit coupling strengths. These model compounds exhibit slightly smaller couplings than the theoretical values, probably due to a combination of vibrational averaging and nonideal scaling factors for the homonuclear decoupling sequences.

Upon membrane binding, the $\text{C}\alpha$ – $\text{H}\alpha$ order parameters decrease to $0.88–0.93$, which correspond to rms amplitudes of $16–12^\circ$. This represents bond fluctuations over a solid angle that is $2.2–3.5$ times larger than that of the soluble protein. The enhanced mobility of colicin associated with membrane binding was confirmed by the static ^{15}N spectra. The ^{15}N CSAs of the membrane-bound colicin Ia channel domain exhibit a 5% reduction from the soluble state. If the

soluble colicin ^{15}N spectrum is taken to be approximately in the rigid limit, then this 5% reduction translates into an rms amplitude of $\sim 10^\circ$ for the backbone of the membrane-bound colicin (22, 34, 35).

The significant backbone angular excursion ($12–16^\circ$) of the membrane-bound colicin Ia channel domain differs from the behavior of bacteriorhodopsin and fd coat protein. ^2H and ^{13}C NMR showed that the bacteriorhodopsin backbone is mostly rigid except for a few “surface residues” and the C-terminus (28, 29, 31). For the fd coat protein, which is significantly smaller than the colicin Ia channel domain, most backbone sites exhibit ^{15}N spectra that are indicative of small-amplitude librational motions with semiangles of only $5–10^\circ$ (36).

(B) *Side Chain Motions.* The side chains of the colicin Ia channel domain exhibit more drastically reduced dipolar couplings, indicating that they execute larger-amplitude reorientations than the backbone. The TEASE ^{13}C -labeling protocol allowed us to probe the dynamics of the Val β and Leu β and γ segments. In the soluble state, the order parameters for the Val $\text{C}\beta$ and Leu $\text{C}\beta$ and $\text{C}\gamma$ segments are $0.87–0.88$. These values correspond to rms amplitudes of 17° and 16° , respectively.

The motion of the Val $\text{C}\beta$ site can be modeled as a combination of the wobbling of the $\text{C}\alpha$ segment and discrete jumps around the $\text{C}\alpha$ – $\text{C}\beta$ bond. Assuming fast jumps among the three Val χ_1 isomers ($+180^\circ$, -60° , $+60^\circ$), the reduction of the $\text{C}\beta$ – $\text{H}\beta$ order parameter from the $\text{C}\alpha$ – $\text{H}\alpha$ value reflects the equilibrium populations of the three sites (67, 68). Equal populations would reduce the C–H couplings of the β -segment by a factor of $1/3$ from that of the α -segment. The experimental reduction factor of ~ 0.88 corresponds to a population distribution of about 90:5:5, assuming that the two minor rotamers, $\chi_1 = -60^\circ$ and $\chi_1 = +60^\circ$, are equally populated. In comparison, no significant order parameter change was observed between the Leu β and γ sites ($S = 0.88$ and 0.87 , respectively), indicating that the χ_2 angle of Leu residues is essentially rigid. This is consistent with the compact packing of colicin Ia in the soluble form, as it limits the space available for discrete jump motions of the bulkier Leu side chains.

Upon membrane binding, the valine and leucine side chains acquire significantly greater mobility: C–H order parameters of $0.60–0.75$ were measured, which translate into rms amplitude fluctuations of $29–23^\circ$. The order parameters were scaled by a factor of $0.69–0.85$ from the soluble state, compared to 0.9 for the backbone sites. In other words, membrane binding preferentially increases the motional amplitudes of the side chains over the backbone. In addition, the dynamic gradients along the leucine and valine side chains are somewhat different between the two states of the protein. While the valine α -to- β order parameter reduction (0.83 , corresponding to a population distribution of 88:6:6 for the three rotamers) is similar to that observed in the soluble colicin, the Leu β -to- γ order parameter reduction is increased to 0.90 . Since X-ray crystallography showed that only two of the nine rotamers, with χ_2 torsion angles of 180° and 60° , are significantly populated in leucyl-containing peptides (69), we used a two-site jump model to calculate the population distribution between the two conformers and found it to be 93:7. Similar side chain disorder has also been

observed in collagen and attributed to discrete jumps (21, 32, 69).

The large side chain mobility distinguishes the membrane-bound colicin Ia channel domain from bacteriorhodopsin, which was found to exhibit no fast motion around the valine C α –C β bond (27). The side chain disorder of the membrane-bound colicin resembles that of the fd coat protein (34, 35) and small membrane peptides in liquid-crystalline bilayers (37–39, 70). Similarly, it has been shown that about 60% of the lysine residues in colicin E1 channel domain have high mobility (19).

The increased disorder in the membrane-bound colicin Ia channel domain was confirmed by the ^1H – ^1H dipolar couplings. All ^1H cross sections of WISE spectra show significantly smaller line widths for the membrane-bound sample than for the soluble protein (Figure 5). Consistent with the C–H coupling results, the H–H order parameters decrease more for the side chains than for the backbone sites. The ratios of the H–H couplings between the membrane-bound and soluble samples are lower than for the corresponding C–H dipolar couplings. This can be understood by considering the multiple ^1H – ^1H couplings. For instance, a methine proton coupled to methyl protons in a neighboring segment would be influenced by the fast methyl group rotation, which is an additional line narrowing mechanism that is absent in the C–H coupling experiments. This extra degree of motional freedom explains the particularly drastic coupling reduction observed for Val C β and Leu C γ , both of which are directly bonded to a methyl group.

The calculation of the rms amplitude of motion from the order parameters provides an informative picture of protein dynamics without any assumptions about the motional model. The only approximation is the Taylor expansion of $\langle \sin \theta \rangle \approx \langle \theta \rangle$, which restricts the analysis to relatively small reorientation angles. However, for the lowest order parameter of 0.6 (rms amplitude of 29°), the difference between $\sin \theta$ and θ is only ~4%, indicating that this analysis is adequate for the most mobile colicin side chains. Alternatively, the CH order parameters can be converted to angular excursions of the C–H bond vector using motional models frequently applied for the interpretation of solution NMR relaxation data (1). Models such as wobbling in a cone or Gaussian axial fluctuation may provide a more instructive picture of molecular processes but also require more assumptions and adjustable parameters. The current analysis highlights the drastic increase in colicin mobility upon membrane binding without relying on specific motional models.

Fast motions such as those in colicin were also reported by molecular dynamics simulations of peptides in lipid bilayers (71, 72). There, the motions were typically considered to be wobbling and librational motions for the backbone and jump motions for the side chains, consistent with our treatment. More quantitative information about the motional geometry may be obtained from ^2H NMR of site-specifically-labeled samples (1, 73).

Our order parameter analyses yield a coarse-resolution dynamics map of the colicin Ia channel domain. Since single-residue resolution is limited in the ^{13}C spectra, and only amino acid type resolution is available, the measured order parameters represent the average values over all residues of the same type. Based on the crystal structure of the soluble colicin (42) and our TEASE labeling protocol, about 80%

of the labeled amino acids (Ala, Ser, Val, Leu, Phe, Tyr, and Trp) reside in α -helices in the soluble state. While membrane binding alters the helix boundaries and helix lengths to some extent (Huster et al., submitted for publication), the current experiments still represent the average dynamics of the helices in the protein.

Microsecond Time Scale Motions in Colicin. Measurement of the motionally averaged dipolar couplings provides the upper limit to the correlation times of the motions. More quantitative correlation times can be obtained from relaxation time measurements. Previous laboratory-frame relaxation time and NOE measurements have found correlation times of 50 ps to a few nanoseconds in other membrane proteins and peptides (8, 32, 36). However, few studies have characterized the microsecond time scale motions in solid proteins and polymers (62, 74). Here, we used the ^1H $T_{1\rho}$ relaxation rates to probe motions with correlation times of about 10 $^{-6}$ s in colicin. The Lee–Goldburg spin-lock experiment yields site-resolved $T_{1\rho}$ values, since ^1H spin diffusion, which homogenizes the relaxation process among many sites, was suppressed. We obtained relaxation times of 7–15 and 3–9 ms for the soluble and membrane-bound colicin, respectively. The latter is significantly shorter than the $T_{1\rho}$'s of rigid crystalline compounds, confirming the larger mobility of the membrane-bound colicin Ia channel domain. Since the measured $T_{1\rho}$ values change with the spin-lock field strengths, the motional correlation times must reside near the $T_{1\rho}$ minimum. Using the ratio of two relaxation times at two spin-lock fields, we obtained an average correlation time of about 0.8 μs for the soluble colicin, and 1.2 μs for the membrane-bound protein.

Which motions occur on the 1 μs time scale? These can include transitions between conformational substates and small-amplitude reorientations of entire helices. For instance, backbone reorientations around helical axes with correlation times of less than 1 μs have been reported for collagen (69). Microsecond time scale motions have also been revealed from ^2H NMR relaxation and line shape analysis of hydrated crystalline lysozyme (66). The microsecond time scale motions in the soluble state of the colicin Ia channel domain could provide the flexibility for the conformational changes required for inserting into the membrane. In the membrane-bound state, the microsecond motions would agree well with the extended helix array model (18). The helix array is flexible, and interhelix interactions that would stabilize the tertiary structure are mostly lost. Thus, the various helices of the membrane-associated colicin are largely uncorrelated and may undergo independent small-angle reorientations in the bilayer. These helix reorientations can be around the bilayer normal, or can be rocking motions in and out of the plane of the bilayer. Small membrane peptides such as gramicidin have also been shown to exhibit microsecond motions in the fluid membrane (40, 75). But to our best knowledge, the colicin Ia channel domain is the largest membrane protein studied so far by NMR to exhibit abundant dynamics on this relatively slow time scale.

Millisecond Time Scale Colicin Dynamics. We searched for millisecond time scale motions in the colicin Ia channel domain using the ^{13}C -detected ^{15}N CODEX experiment. Our data show that no motions occur between 1 and 400 ms in either the soluble or the membrane-bound state of the protein. While it is not surprising that the compact soluble colicin Ia

channel domain does not execute millisecond motions (54), one might expect the membrane-bound protein to exhibit slow motions due to rotational diffusion of this relatively large molecule in the bilayer. However, a simple estimate suggests that rotational diffusion of the colicin Ia channel domain should be much faster than the millisecond time scale of the exchange experiment. According to the Saffman–Delbrück theory (76, 77), the rotational diffusion rate (D_R) of a macromolecule with a cylindrical shape of radius a immersed in the membrane to a depth of h is given by

$$D_R = \frac{1}{\tau_R} = \frac{k_B T}{4\pi\eta a^2 h} \quad (5)$$

where k_B is the Boltzmann constant, T is the temperature, and η is the membrane viscosity. The membrane-bound colicin Ia channel domain can be considered as a disk subtending an area of 4200 \AA^2 on the bilayer surface (18), which gives a radius of $\sim 37 \text{ \AA}$. Assuming the protein to be immersed in the bilayer by 10 \AA , and the membrane viscosity to be 1 P , we obtain a rotational diffusion correlation time τ_R of $40 \mu\text{s}$. This time scale falls right between the time windows of the CODEX and the $T_{1\rho}$ experiment; thus, this motion was not probed by our experiments. While this estimate is crude, it yields the same order of magnitude of the correlation times (20 – $400 \mu\text{s}$) as those found in several membrane proteins, including rhodopsin, bacteriorhodopsin, and cytochrome P-450 (78).

Significance of Increased Dynamics of Membrane-Bound Colicin. The function of the colicin Ia channel domain as a bactericidal protein requires it to undergo a series of conformational transitions in order to adapt to different dielectric environments and electrical conditions. This suggests that the protein is inherently more flexible than average membrane proteins. The observed large-amplitude motions in the backbone and side chains of the membrane-bound colicin, beyond what is typically found in other membrane proteins, and beyond what we detected in the soluble colicin, support this view. These large-amplitude motions can be important for reducing the free-energy barrier for the next conformational change, to the open-channel state. More specifically, the loose and mobile structure of the closed channel may facilitate the transmembrane movement of major parts of the protein during channel opening (4, 5). The higher mobility of the membrane-bound colicin Ia channel domain compared to other membrane proteins also supports the hypothesis of an extended helix structure as a precursor state for channel formation (17, 18).

Collisions with lipid molecules in the liquid-crystalline bilayer (38, 79, 80) are likely to be the main sources of the observed enhanced dynamics of the membrane-bound colicin. Lipid lateral diffusion, uniaxial rotational diffusion, and collective thermal motions can induce the sub-microsecond to microsecond motions observed in the membrane-bound colicin. Moreover, the extended structure believed to be formed by colicin at the membrane–water interface will increase the interaction between the lipids and the protein. The dependence of protein dynamics on membrane structure has been previously demonstrated by NMR studies of small membrane peptides as a function of the phase state of the lipid bilayer (38). It is also supported by molecular dynamics simulations of model peptides in lipid membranes (71), which

showed that side chains buried in the nonpolar membrane environment are more mobile on the picosecond time scale than the water-accessible side chains. Conversely, the conformational dynamics of the lipid molecules can also be increased by interactions with the protein. The decreased ^2H order parameters of the lipids in the presence of colicin (Huster et al., submitted for publication) provide corroborating evidence that colicin, by acting as a spacer between the lipid headgroups, induces larger-amplitude motions in the lipid acyl chains.

Finally, the preferential increase of mobility of the side chains over the backbone in the membrane-bound colicin Ia channel domain is noteworthy. This is consistent with the relatively small changes in the secondary structure content seen in the α -helix and β -sheet filter experiments (Huster et al., submitted for publication). If we combine the NMR results of retained secondary structure, large side chain mobility, and fluctuation of entire helices that makes tertiary structure ill-defined, and if we broadly interpret a “globule” as a well-defined polypeptide backbone without necessarily having a compact shape, then the membrane-bound colicin Ia channel domain exhibits the classical signatures of a molten-globule state. Thus, the molten-globule model may be appropriate for describing the structure of the membrane-bound colicin Ia channel domain.

CONCLUSIONS

Using solid-state NMR spectroscopy, we have measured a number of nuclear spin interactions in the colicin Ia channel domain in order to examine the dynamic differences between the soluble and the membrane-bound states of the protein. In the soluble state, the colicin Ia channel domain executes small-amplitude librational motions in the backbone (rms amplitudes of 10 – 0°) and larger-amplitude jump motions in the side chains (17 – 16°). These rms amplitudes are determined from the reduced C–H, H–H dipolar couplings and the ^{15}N chemical shift anisotropies. Upon membrane binding, the motional amplitudes for both the backbone and side chains increase significantly. Backbone C–H order parameters of 0.88 – 0.93 were obtained, corresponding to rms amplitudes of 16 – 12° . For the side chains, order parameters of 0.60 – 0.75 were measured and yielded rms amplitudes of 29 – 23° . Thus, membrane binding preferentially increases the side chain mobility over the backbone. Further, a small increase in the dynamic gradients along the Leu and Val side chains was observed in the membrane-bound colicin. These reflect two- or three-site jumps with unequal populations. While these order parameters likely reflect fast motions on the sub-nanosecond time scale, we found that colicin also possesses significant microsecond motions that are more pronounced in the membrane-bound state than in the soluble state. This is manifested by the ^1H $T_{1\rho}$ relaxation times, which are 7 – 15 ms for the soluble protein and 3 – 9 ms for the membrane-bound protein. Based on the $T_{1\rho}$ ratios at different spin-lock field strengths, we found correlation times of about $0.8 \mu\text{s}$ for the soluble state and $1.2 \mu\text{s}$ for the membrane-bound state. Finally, both states of the colicin Ia channel domain are completely immobile on the millisecond time scale.

Comparing the dynamic data of this study with previous work on other membrane proteins, we conclude that the

colicin Ia channel domain has enhanced conformational flexibility than membrane proteins of comparable or even smaller sizes. The increased dynamics is consistent with the loss of the compact structure of the protein upon membrane binding. Contrary to other membrane-bound proteins, the helical colicin Ia channel domain probably covers a large membrane surface as a helical array. The weakening of the interhelix interactions would lead to an increase in segmental mobility, which can manifest as small rocking motions of the helices in and out of the lipid–water interface, or restricted rotations around the bilayer normal. With this extended structure, collisions with lipid molecules would also be more frequent, further increasing the mobility of the membrane-bound protein. We hypothesize that the enhanced dynamics of the membrane-bound colicin Ia channel domain are a prerequisite for channel opening in the presence of a voltage gradient.

ACKNOWLEDGMENT

We thank Dr. K. Jakes (Albert Einstein College of Medicine) for providing the isotopically labeled colicin sample and Prof. K. Schmidt-Rohr for helpful discussions on NMR order parameters.

REFERENCES

- Palmer, A. G., III, Williams, J., and McDermott, A. (1996) *J. Phys. Chem.* **100**, 13293–13310.
- Akke, M., Liu, J., Cavanagh, J., Erickson, H. P., and Palmer, A. G., III (1998) *Nat. Struct. Biol.* **5**, 55–59.
- Kay, L. E. (1998) *Nat. Struct. Biol.* **5 Suppl.**, 513–517.
- Slatin, S. L., Qiu, X. Q., Jakes, K. S., and Finkelstein, A. (1994) *Nature* **371**, 158–161.
- Qiu, X. Q., Jakes, K. S., Kienker, P. K., Finkelstein, A., and Slatin, S. L. (1996) *J. Gen. Physiol.* **107**, 313–328.
- Cha, A., Snyder, G. E., Selvin, P. R., and Bezanilla, F. (1999) *Nature* **402**, 809–813.
- Glauner, K. S., Mannuzzu, L. M., Gandhi, C. S., and Isacoff, E. Y. (1999) *Nature* **402**, 813–817.
- North, C. L., and Cross, T. A. (1995) *Biochemistry* **34**, 5883–5895.
- Prosser, R. S., Davis, J. H., Dahlquist, F. W., and Lindorfer, M. A. (1991) *Biochemistry* **30**, 4687–4696.
- Litman, B. J., and Mitchell, D. C. (1996) *Lipids* **31**, S-193–S-197.
- Stroud, R. (1995) *Curr. Opin. Struct. Biol.* **5**, 514–520.
- Cramer, W. A., Heymann, J. B., Schendel, S. L., Deriy, B. N., Cohen, F. S., Elkins, P. A., and Stauffacher, C. V. (1995) *Annu. Rev. Biophys. Biomol. Struct.* **24**, 611–641.
- Laake, J. H., Gonzalez-Manas, J. M., van der Goot, F. G., and Pattus, F. (1992) *FEBS Lett.* **307**, 26–29.
- Parker, M. W., Tucker, A. D., Tsernoglou, D., and Pattus, F. (1990) *Trends Biochem. Sci.* **15**, 126–129.
- van der Goot, F. G., Gonzalez-Manas, J. M., Laake, J. H., and Pattus, F. (1991) *Nature* **354**, 408–410.
- Lindeberg, M., Zakharov, S. D., and Cramer, W. A. (2000) *J. Mol. Biol.* **295**, 679–692.
- Zakharov, S. D., Lindeberg, M., and Cramer, W. A. (1999) *Biochemistry* **38**, 11325–11332.
- Zakharov, S. D., Lindeberg, M., Griko, Y., Salamon, Z., Tollin, G., Prendergast, F. G., and Cramer, W. A. (1998) *Proc. Natl. Acad. Sci. U.S.A.* **95**, 4282–4287.
- Kumashiro, K. K., Schmidt-Rohr, K., Murphy, O. J., III, Ouellette, K. L., Cramer, W. A., and Thompson, L. K. (1998) *J. Am. Chem. Soc.* **120**, 5043–5051.
- Kienker, P. K., Qiu, X., Slatin, S. L., Finkelstein, A., and Jakes, K. S. (1997) *J. Membr. Biol.* **157**, 27–37.
- Torchia, D. A. (1984) *Annu. Rev. Biophys. Bioeng.* **13**, 125–144.
- Opella, S. J. (1986) *Methods Enzymol.* **131**, 327–361.
- Siminovitch, D. J. (1998) *Biochem. Cell Biol.* **76**, 411–422.
- Torchia, D. A., and Szabo, A. (1985) *J. Magn. Reson.* **64**, 135–141.
- Vold, R. R., and Vold, R. L. (1991) in *Advances in magnetic and optical resonance* (Warren, W. S., Ed.) pp 85–171, Academic Press, San Diego.
- Spiess, H. W. (1978) in *NMR basic principles and progress* (Diehl, P., Fluck, E., and Kosfeld, R., Eds.) pp 55–214, Springer-Verlag, Berlin.
- Oldfield, E., Kinsey, R. A., and Kintanar, A. (1982) *Methods Enzymol.* **88**, 310–325.
- Keniry, M. A., Gutowsky, H. S., and Oldfield, E. (1984) *Nature* **307**, 383–386.
- Bowers, J. L., and Oldfield, E. (1988) *Biochemistry* **27**, 5156–5161.
- Saito, H., Tuzi, S., Yamaguchi, S., Tanio, M., and Naito, A. (2000) *Biochim. Biophys. Acta* **1460**, 39–48.
- Herzfeld, J., Mulliken, C. M., Siminovitch, D. J., and Griffin, R. G. (1987) *Biophys. J.* **52**, 855–858.
- Keniry, M. A., Kintanar, A., Smith, R. L., Gutowsky, H. S., and Oldfield, E. (1984) *Biochemistry* **23**, 288–298.
- Lewis, B. A., Harbison, G. S., Herzfeld, J., and Griffin, R. G. (1985) *Biochemistry* **24**, 4671–4679.
- Leo, G. C., Colnago, L. A., Valentine, K. G., and Opella, S. J. (1987) *Biochemistry* **26**, 854–862.
- Colnago, L. A., Valentine, K. G., and Opella, S. J. (1987) *Biochemistry* **26**, 847–854.
- Cross, T. A., and Opella, S. J. (1982) *J. Mol. Biol.* **159**, 543–549.
- Koenig, B. W., Ferretti, J. A., and Gawrisch, K. (1999) *Biochemistry* **38**, 6327–6334.
- Mueller, L., Frey, M. H., Rockwell, A. L., Giersch, L. M., and Opella, S. J. (1986) *Biochemistry* **25**, 557–561.
- Lee, K. C., Huo, S., and Cross, T. A. (1995) *Biochemistry* **34**, 857–867.
- Prosser, R. S., and Davis, J. H. (1994) *Biophys. J.* **66**, 1429–1440.
- Hong, M., and Jakes, K. S. (1999) *J. Biomol. NMR.* **14**, 71–74.
- Wiener, M., Freymann, D., Ghosh, P., and Stroud, R. M. (1997) *Nature* **385**, 461–464.
- Hope, M. J., Bally, M. B., Webb, G., and Cullis, P. R. (1985) *Biochim. Biophys. Acta* **812**, 55–65.
- Smith, P. K., Krohn, R. I., Hermanson, G. T., Mallia, A. K., Gartner, F. H., Provenzano, M. D., Fujimoto, E. K., Goeke, N. M., Olson, B. J., and Klenk, D. C. (1985) *Anal. Biochem.* **150**, 76–85.
- Bennett, A. E., Rienstra, C. M., Auger, M., Lakshmi, K. V., and Griffin, R. G. (1995) *J. Chem. Phys.* **103**, 6951–6958.
- Kolbert, A. C., de Groot, H. J. M., Levitt, M. H., Munowitz, M. G., Roberts, J. E., Harbison, G. S., Herzfeld, J., and Griffin, R. G. (1990) in *Multinuclear magnetic resonance in liquids and solids—chemical applications* (Granger, P., and Harris, R. K., Eds.) pp 339–354, Kluwer Academic Publishers, Dordrecht.
- Rienstra, C. M., Hatcher, M. E., Mueller, L. J., Sun, B., Feisik, S. W., and Griffin, R. G. (1998) *J. Am. Chem. Soc.* **120**, 10602–10612.
- Rhim, W.-K., Elleman, D. D., and Vaughan, R. W. (1973) *J. Chem. Phys.* **59**, 3740–3749.
- Bielecki, A., Kolbert, A. C., and Levitt, M. H. (1989) *Chem. Phys. Lett.* **155**, 341–345.
- Vinogradov, E., Madhu, P. K., and Vega, S. (1999) *Chem. Phys. Lett.* **314**, 443–450.
- Hong, M., Gross, J. D., Rienstra, C. M., Griffin, R. G., Kumashiro, K. K., and Schmidt-Rohr, K. (1997) *J. Magn. Reson.* **129**, 85–92.
- Hong, M., Gross, J. D., and Griffin, R. G. (1997) *J. Phys. Chem.* **101**, 5869–5874.
- Schmidt-Rohr, K., Clauss, J., and Spiess, H. W. (1992) *Macromolecules* **25**, 3273–3277.
- deAzevedo, E. R., Kennedy, S. B., and Hong, M. (2000) *Chem. Phys. Lett.* **321**, 43–48.

55. deAzevedo, E. R., Hu, W.-G., Bonagamba, T. J., and Schmidt-Rohr, K. (1999) *J. Am. Chem. Soc.* **121**, 8411–8412.
56. Hing, A. W., Vega, S., and Schaefer, J. (1992) *J. Magn. Reson.* **96**, 205–209.
57. Metz, G., Wu, X., and Smith, S. O. (1994) *J. Magn. Reson., Ser. A* **110**, 219–227.
58. van Rossum, B.-J., de Groot, C. P., Ladizhansky, V., Vega, S., and de Groot, H. J. M. (2000) *J. Am. Chem. Soc.* **122**, 3465–3472.
59. Mehring, M. (1983) *Principles of high-resolution NMR in solids*, Springer-Verlag, Heidelberg.
60. Schmidt-Rohr, K., and Spiess, H. W. (1994) *Multidimensional solid-state NMR and polymers*, Academic Press, San Diego.
61. Opella, S. J., Stewart, P. L., and Valentine, K. G. (1987) *Q. Rev. Biophys.* **19**, 7–49.
62. Schaefer, J., Stejskal, E. O., and Buchdahl, R. (1977) *Macromolecules* **10**, 384–405.
63. Brüschweiler, R. (1994) in *Nuclear magnetic resonance probes of molecular dynamics* (Tycko, R., Ed.) pp 301–334, Kluwer Academic Publishers, Dordrecht.
64. Lipari, G., and Szabo, A. (1982) *J. Am. Chem. Soc.* **104**, 4546–4559.
65. Cole, H. B. R., and Torchia, D. A. (1991) *Chem. Phys.* **158**, 271–281.
66. Mack, J. W., Usha, M. G., Long, J., Griffin, R. G., and Wittebort, R. J. (2000) *Biopolymers* **53**, 9–18.
67. Blume, A., Rice, D. M., Wittebort, R. J., and Griffin, R. G. (1982) *Biochemistry* **21**, 6220–6230.
68. Speyer, J. B., Weber, R. T., Das Gupta, S. K., and Griffin, R. G. (1989) *Biochemistry* **28**, 9569–9574.
69. Batchelder, L. S., Sullivan, C. E., Jelinski, L. W., and Torchia, D. A. (1982) *Proc. Natl. Acad. Sci. U.S.A.* **79**, 386–389.
70. Lee, K. C., and Cross, T. A. (1994) *Biophys. J.* **66**, 1380–1387.
71. Belohorcova, K., Davis, J. H., Woolf, T. B., and Roux, B. (1997) *Biophys. J.* **73**, 3039–3055.
72. Berneche, S., Nina, M., and Roux, B. (1998) *Biophys. J.* **75**, 1603–1618.
73. Wittebort, R. J., Olejniczak, E. T., and Griffin, R. G. (1987) *J. Phys. Chem.* **86**, 5411–5420.
74. Shaw, W. J., Long, J. R., Campbell, A. A., Stayton, P. S., and Drobny, G. P. (2000) *J. Am. Chem. Soc.* **122**, 7118–7119.
75. Pauls, K. P., MacKay, A. L., Soderman, O., Bloom, M., Tanjea, A. K., and Hodges, R. S. (1985) *Eur. Biophys. J.* **12**, 1–11.
76. Saffman, P. G., and Delbrück, M. (1975) *Proc. Natl. Acad. Sci. U.S.A.* **72**, 3111–3113.
77. Tamm, L. K. (1991) *Biochim. Biophys. Acta* **1071**, 123–148.
78. Cherry, R. J. (1979) *Biochim. Biophys. Acta* **559**, 289–327.
79. Huster, D., and Gawrisch, K. (2000) in *Lipid bilayers: structure and interactions* (Katsaras, J., and Gutberlet, T., Eds.) pp 109–125, Springer-Verlag, Berlin.
80. Feller, S. E., Huster, D., and Gawrisch, K. (1999) *J. Am. Chem. Soc.* **121**, 8963–8964.

BI0027231